ISSN: 2710-0588

Unified Boundary Control for Dual Bridge Series Resonant DC-DC Converter

Guo Chen, Hai Li, and Yong Li

School of Mechatronic Engineering, Zhongshan Polytechnic, Zhongshan 528400, China

Abstract

In this paper, the TPS control with certain unified boundary condition is applied to a DBSRC. The control strategy is unified for the whole variation range of load, input/output voltage and with simple calculation. By using this unified boundary control, the circulating energy is minimized significantly. A wide soft switching operation range can be achieved. The steady-state analysis of the DBSRC will be performed using fundamental harmonics approximation (FHA) approach. The design principle for unified boundary control is then discussed. A design example based on the analysis results is presented and then verified through simulation and experiment.

Keywords

DC-DC Conversion, ZVS, Full-bridge Converter, TPS Modulation.

1. Introduction

Due to the problems of global warming and energy crisis, the technology and application of renewable energy have been widely studied [1-2]. A high frequency (HF) isolated bidirectional DC-DC converter (IBDC) is a key power interface for renewable energy systems. Dual-active-bridge (DAB) DC-DC converter was initially proposed in [3-6], which is typical type of IBDC. A DAB converter consists of two active full bridges linked through a high frequency (HF) transformer and a series inductor. DAB converters have shown many competitive advantages such as high power density, high reliability, high efficiency, symmetrical circuit structure, simple control strategies, and so on. Since a DAB converter is operated with high switching frequency, the size of reactive component and HF related noise will be reduced. The double-bridge series resonant converter (DBSRC) is a resonant version of DAB and also a powerful choice for achieving high power density [7-8]. With the high frequency, the size of reactive component of DBSRC will be small too. Due to the resonance characteristics, there are some extra features in DBSRC. In this paper, the research would be performed on a HF DBSRC.

Until now, there are four types of control schemes mainly used for DAB and DBSRC converters [4]. The most commonly used scheme is SPS because it has the advantages of simple controller and easy implementation by digital control. However, in this method, with the variation of voltage gain and load level, the circulation energy becomes much higher, and its efficiency is greatly lowered. EPS control is an improved version with one more controllable phase-shift angel. Compared with SPS control, EPS control can reduce circulating energy and expand soft-switching range. However, when the power flow direction is changed, the working modes of the two bridges need to be exchanged to reduce circulating energy. DPS control is easier to implement than EPS control, because the inner phase-shift angles in two bridges are equal. With DPS control, the converter dynamic performance may be improved. However, the improvement of efficiency is not significantly in some operating regions. TPS is a unified form of phase-shift control, while SPS, DPS and EPS can also be regarded as special cases of TPS control. The TPS control is the most complex but flexible control scheme.

ISSN: 2710-0588

Taking into account of flexibility, powerfulness and complexity of four control schemes, in this paper, the TPS control scheme is adopted. To address the problem of complex calculation, complex working mode classification and narrow softer switching region, the TPS control with certain unified boundary condition will be applied to a DBSRC. The control strategy is flexible, unified and with simple calculation. The steady-state analysis of the DBSRC will be performed using fundamental harmonics approximation approach at first. After that, the design principle for unified boundary control is discussed. As an example, the application of unified boundary TPS control has been examined in a dual-bridge series resonant converter (DBSRC), which is able to suppress circulating energy and maintain soft switching operation for all switches at variation of converter gain and load.

2. Analysis and Design of DBSRC with TPS Control

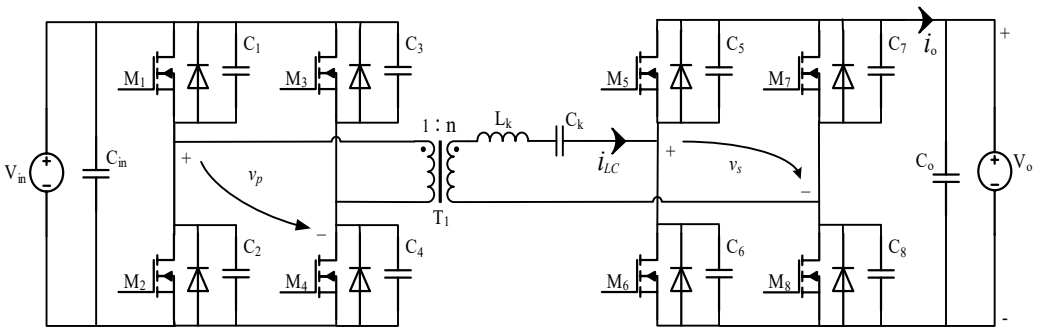

Fig. 1 Basic topology of a dual-bridge series resonant converter.

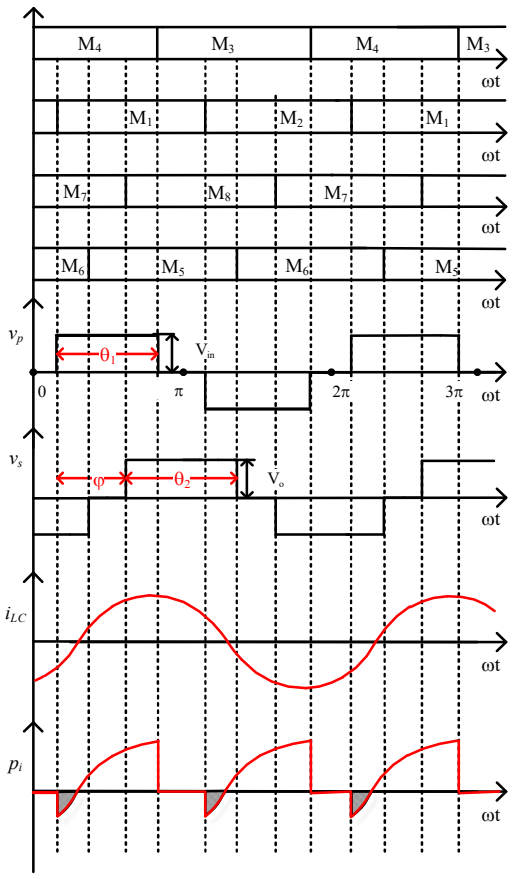

Fig. 2 Typical operating waveforms of the DBSRC under conventional TPS control with all switches in ZVS.

ISSN: 2710-0588

Fig. 1 shows the basis topology configuration of a DBSRC. Both the primary side and the secondary are active full-bridges. The two symmetric full-bridges are connected by a series LC-type resonant tank and a high-frequency transformer T_1. The two voltage sources V_{in} and V_o are the primary side voltage and secondary side voltage, respectively. The primary side bridge is implemented by four switches M_1-M_4, and the secondary side bridge is constructed by four switches M_5-M_8. C_1-C_8 are the output parasitic capacitors of switches M_1-M_8, respectively. C_{in} and C_o are filter capacitors on the input side and output side, respectively. The leakage inductance of the HF transformer is utilized as part of resonant inductance L_k. The series capacitor C_k used in the resonant tank will help in preventing the transformer from saturation. High-frequency (HF) transformer T_1 with a turns ratio of 1:n provides functions of electrical isolation and voltage level conversion.

The operation principle of conventional TPS control is shown in Fig. 2. Energy is exchanged bidirectionally between the primary side voltage source Vin and the secondary voltage source Vo due to the symmetric structure of DBSRC. The power transfer from the primary side to the secondary side is defined as a forward power flow. It is seen that all switches are operating alternatively at almost 50% duty cycle with necessary dead-time. Three phase-shift angles are defined here for bidirectional power regulation. The inner-bridge phase-shift θ1 is defined as the phase-shift by which the driver signal of M4 leads that of M1 in the primary side bridge. θ1 is in the range of [0,π]. The inner-bridge phase-shift θ2 is defined as the phase-shift by which the driver signal of M8 lags that of M5 in the secondary side bridge. The range of θ2 is [0,π]. Thus, the obtained two high frequency ac voltages vp and vs are no longer traditional square-wave voltage due to the existence of internal phase-shift. With TPS control, three-level PWM waveforms are generated in both the primary and secondary bridge. The external phase-shift φ is defined as the phase-shift by which the driver signal of M1 leads that of M8. The external phase-shift φ can also be defined as the phase-shift by which the rising edge of vp from zero to high level leads to that of vs during one switching period. The range of φ depends on the direction of power and the values of θ1 and θ2. The instantaneous input power pi is discontinuous and can be controlled by the combination of three phase-shift angles.

When the switching frequency is close to the resonant frequency, fundamental harmonics approximation (FHA) analysis is adopted for the steady state analysis with simplified calculation and acceptable accuracy. The obtained equations can be used for a quick initial converter design with enough accuracy. All parameters have been reflected to the secondary side (denoted by a superscript "′", if the parameter is on the primary side). In order to obtain normalized equations, the following base values are chosen:

$$V_B = nV_{in}, Z_B = \frac{V_o^2}{P_R}, I_B = \frac{V_B}{Z_B}, f_B = f_r = \frac{1}{2\pi\sqrt{L_k C_k}}, P_B = \frac{V_B^2}{Z_B} \tag{1}$$

where fr is the series resonance frequency, PR is the rated output power.

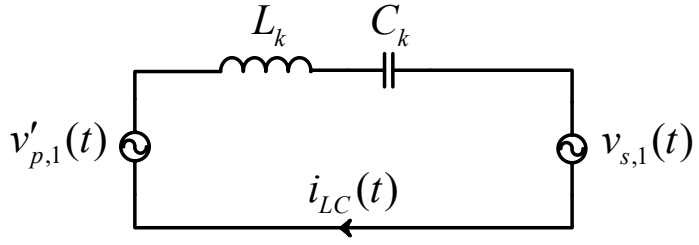

Fig. 3 Equivalent circuit for fundamental components in time domain.

ISSN: 2710-0588

In Fig. 3, the steady-state equivalent circuit of DBSRC is given. The normalized two voltage sources of v′p and vs in time domain with only fundamental components can be expressed as:

$$v'_{p,1pu}(\omega_s t) = \frac{4}{\pi}\sin\frac{\theta_1}{2}\sin(\omega_s t) \tag{2}$$

$$v_{s,1pu}(\omega_s t) = \frac{4M}{\pi}\sin\frac{\theta_2}{2}\sin\left[\omega_s t - \left(\varphi + \frac{\theta_2 - \theta_1}{2}\right)\right] \tag{3}$$

where the converter gain M is defined as $M = \frac{V_o}{nV_{in}}$, ωs is the switching angular frequency. It is seen from (3) that the fundamental component of v'_p leads that of vs by a phase-shift angle of $\varphi + \frac{\theta_2 - \theta_1}{2}$.

The normalized impedance of the resonant tank can be written as:

$$X_{s,pu} = (\omega_s L_k - \frac{1}{\omega_s C_k}) / Z_B = Q(F - 1/F) \tag{4}$$

where rated load quality factor Q is defined as $Q = \frac{\omega_r L_k}{Z_B} = \frac{1}{\omega_r C_k Z_B}$, the normalized switching frequency F can be expressed as $F = \frac{\omega_s}{\omega_r}$, and ωr is the resonant angular frequency.

Then the normalized resonant tank current $i_{LC,pu}$ in time domain with only fundamental component can be found as:

$$i_{LC,pu}(\omega_s t) = \frac{4\left[M\sin\frac{\theta_2}{2}\cos(\omega_s t - \phi) - \sin\frac{\theta_1}{2}\cos(\omega_s t)\right]}{\pi X_{s,pu}} \tag{5}$$

By using (5), the normalized root-mean-square (rms) current $I_{LCr,pu}$ is given as:

$$I_{LCr,pu} = \frac{\sqrt{8M^2\sin^2\frac{\theta_2}{2} - 16M\sin\frac{\theta_1}{2}\sin\frac{\theta_2}{2}\cos(\varphi + \frac{\theta_2 - \theta_1}{2}) + 8\sin^2\frac{\theta_1}{2}}}{\pi X_{s,pu}} \tag{6}$$

The normalized resonant tank capacitor peak voltage can be evaluated as follows:

$$V_{Cp,pu} = \frac{\sqrt{16M^2\sin^2\frac{\theta_2}{2} - 32M\sin\frac{\theta_1}{2}\sin\frac{\theta_2}{2}\cos(\varphi + \frac{\theta_2 - \theta_1}{2}) + 16\sin^2\frac{\theta_1}{2}}}{\pi\left(F^2 - 1\right)} \tag{7}$$

ISSN: 2710-0588

Ignoring the circuit loss, the normalized average transferred power with TPS control in a switching cycle can be evaluated from either side of the converter, which can be calculated as:

$$\begin{aligned} P_{o,pu} &= \frac{1}{2\pi}\int_0^{2\pi} v'_{p,1pu}(\omega_s t) i_{LC,pu}(\omega_s t) d\omega_s t \\ &= \frac{8M}{\pi^2 X_{s,pu}} \sin\frac{\theta_1}{2}\sin\frac{\theta_2}{2}\sin(\varphi+\frac{\theta_2-\theta_1}{2}) \end{aligned} \tag{8}$$

3. The Proposed Unified Boundary TPS Control

It can be seen from Fig. 2 that DBSRC operating under conventional TPS control with all switches in ZVS does not guarantee complete elimination of circulating energy (marked by shadow part of instantaneous input power pi). The high circulating current would cause high rms resonant tank current and hence lead to high switches conduction loss. So in this work, the optimization object for selecting a control scheme is to depress circulating energy and, meanwhile, to achieve a wide soft switching operation range. A unified boundary TPS control based on TPS control is proposed to eliminate circulating energy and extend soft switching operation range.

Since unified boundary TPS control is a special case of TPS control, the obtained equations (1)-(8) are suitable for unified boundary TPS control with certain constraints. The constraints can be derived in the following.

To eliminate circulating energy, the HF voltage vp should be in phase with tank current iLC. To realize zero-voltage switching (ZVS) work, the instantaneous resonant tank currents before the turn-on instances of switches are supposed to be high enough to be able to charge/discharge the switches parasitic capacitors completely. To realize zero-current switching (ZCS) work, the instantaneous currents at the turn-on instances of switches are supposed to be zero. Based on above discussion, the following necessary conditions shall be satisfied under Boundary TPS operation.

$$i_{LC,pu}(\frac{\pi-\theta_1}{2}) = \frac{4\left[-\sin^2\frac{\theta_2}{2} + M\sin\frac{\theta_2}{2}\cos(\varphi+\frac{\theta_2}{2})\right]}{\pi X_{s,pu}} = 0 \tag{9}$$

$$i_{LC,pu}(\frac{\pi+\theta_1}{2}) = \frac{4\left[\sin^2\frac{\theta_2}{2} + M\sin\frac{\theta_2}{2}\sin(\varphi-\theta_1+\frac{\theta_2}{2})\right]}{\pi X_{s,pu}} > 0 \tag{10}$$

$$i_{LC,pu}(\varphi+\frac{\pi-\theta_1}{2}) = \frac{4\left[\sin\frac{\theta_1}{2}\sin(\varphi-\frac{\theta_1}{2}) + M\sin^2\frac{\theta_2}{2}\right]}{\pi X_{s,pu}} > 0 \tag{11}$$

$$i_{LC,pu}(\varphi+\frac{\pi-\theta_1}{2}+\theta_2) = \frac{4\left[\sin\frac{\theta_1}{2}\sin(\varphi-\frac{\theta_1}{2}+\theta_2) - M\sin^2\frac{\theta_2}{2}\right]}{\pi X_{s,pu}} = 0 \tag{12}$$

ISSN: 2710-0588

Switches M3 and M4 can work in ZVS if (10) is true; switches M7 and M8 can work in ZVS if (11) is true. Switches M1 and M2 can work in ZCS if (9) is true; switches M5 and M6 can work in ZCS if (12) is true. The statements above are valid for both positive and negative power.

Furthermore, according to the control principle of unified boundary TPS operation modulation, the ranges for three phase angles can be obtained as:

$$\begin{cases} \varphi \le \theta_1 \le \pi \\ \varphi + \theta_2 \le \pi \end{cases} \tag{13}$$

Through solving the soft switching conditions from (9)-(12) under the phase angles ranges in (13), the boundary condition of two angels can be written by

$$\pi = \varphi + \theta_2 \tag{14}$$

Then, substituting (14) into (9) or (12), the quantity relationship of θ1 and θ2 can be expressed as

$$\sin\frac{\theta_1}{2} = \sqrt{M}\,\sin\frac{\theta_2}{2} \tag{15}$$

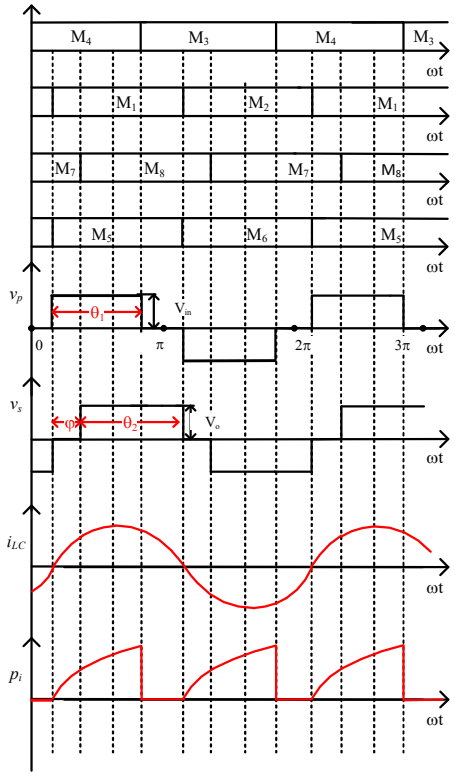

Fig. 4 Typical operating waveforms of the DBSRC under unified boundary TPS control.

Based on the (13)-(15), the working principle of unified boundary TPS control is depicted in Fig. 4. The definitions of three phase shift angles are the same as conventional TPS control. By turning on M1 and M5 simultaneously, the positive rising edge of vp aligns with the negative falling edge of vs. Meanwhile, the turn-on moment of M1 is set at the zero crossing point of

ISSN: 2710-0588

resonant tank current iLC. Therefore, ZVS performance can be accomplished easily for the primary side leading legs switches (M3, M4) and the secondary side lagging legs switches (M7, M8). Meanwhile, the ZCS performance is achieved for the remaining four switches (M1 and M2, M5 and M6). Consequently, it can be concluded that soft switching can be achieved for all the eight switches when the DBSRC converter works in the boundary TPS mode. Additionally, there is no negative part of instantaneous input power pi. Thus, the circulation energy and conduction loss can be minimized.

Based on the principle, under the unified boundary TPS control, the output power can be controlled solely by the external phase-shift φ. The other two phase-shift angles (θ1 and θ2) can be represented by φ from equations (14) and (15). In (8), substituting θ1 and θ2 into φ, the normalized output power $P_{o,pu}$ under unified boundary TPS control can be rewritten as

$$P_{o,pu}=\frac{8M^{\frac{3}{2}}}{\pi^2 X_{s,pu}}\cos^2\frac{\varphi}{2}\cos\left[\arcsin(\sqrt{M}\cos\frac{\varphi}{2})-\frac{\varphi}{2}\right] \tag{16}$$

4. Validation by Simulation and Experiment

4.1. Design Point

To validate the analysis of the unified boundary TPS control, a design example is given firstly. According to the steady-state analysis equations presented in Section II, the approximately optimal parameters needed to be chosen include M (converter gain), F (normalized switching frequency) and Q (rated load quality factor). The specifications of the converter are listed in Table 1.

Table 1. Specification of designed converter

Parameter	Value
Maximum input voltage $V_{in,\max}$	400 V
Minimum input voltage $V_{in,\min}$	360 V
Nominal input voltage $V_{in,\mathrm{n}}$	380 V
Nominal output voltage V_o	120 V
Rated output power P_R	500 W
Switching frequency f_s	100 kHz

In order to obtain high efficiency and optimum performance, the voltage gain at nominal input voltage is selected at unity gain, i.e., $M_n=1$. With the nominal input voltage $V_{in,n}=380$ V and $V_o=120$ V, the primary side reflected input voltage is $V'_{in,n}=V_{in,n}M_n$. Therefore, the turns ratio of high frequency transformer is found as $n=\frac{V_o}{V'_{in,n}}=\frac{12}{38}$.

ISSN: 2710-0588

With the optimal value of $F=1.26$, $Q=1$ at design point selected, the resonant tank parameters can be calculated as:

$$L_k = \frac{QFV_o^2}{\omega_s P_o} = 57.8\,\mu\text{H} \tag{17}$$

$$C_k = \frac{FP_o}{\omega_s Q V_o^2} = 69.6\,\text{nF} \tag{18}$$

4.2. Simulation Results

To verify the proposed unified boundary TPS control strategy, simulations of the design converter were performed in PSIM. The DBSRC to be simulated has the same circuit specification as the designed converter in the last section. Fig. 5-10 illustrate some simulation plots, which were simulated under the full load and 60% load operation at Mmin, Mn and Mmax, respectively. The waveforms shown in the simulations include: vp, vs (two HF AC voltages), iLC (the resonant tank current) and vo (the output voltage). It can be seen from the waveforms of iLC, vp and vs that the circulating current on the both sides are almost zero at full load case and also not significant at 60% load case regardless of the converter voltage gain, which indicates low switches conduction losses and high efficiency. The resonant tank current iLC is near sinusoidal. The output voltage is stable with small voltage ripple. Soft switching can be maintained for all the eight switches at wide load range. Base on the above discussion, the simulation results verify the theoretical analysis.

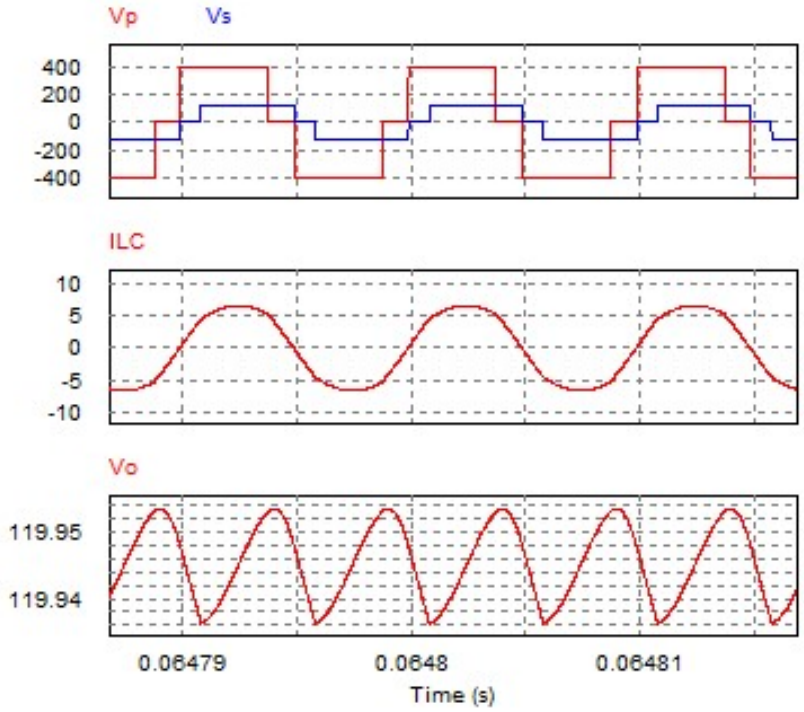

Fig. 5 Simulated waveforms of v_p and v_s, resonant tank current i_{LC}, output volgage V_o for output power P_o=500W (V_{in}=400V, V_o=120V)

ISSN: 2710-0588

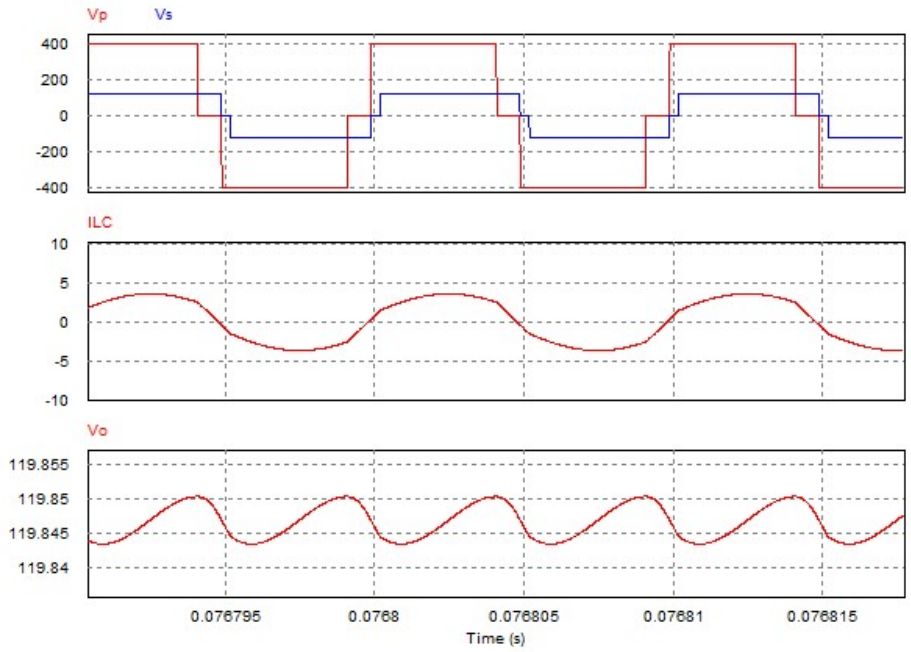

Fig. 6 Simulated waveforms of v_p and v_s, resonant tank current i_{LC}, output volgage V_o for output power P_o=300W (V_{in}=400V, V_o=120V)

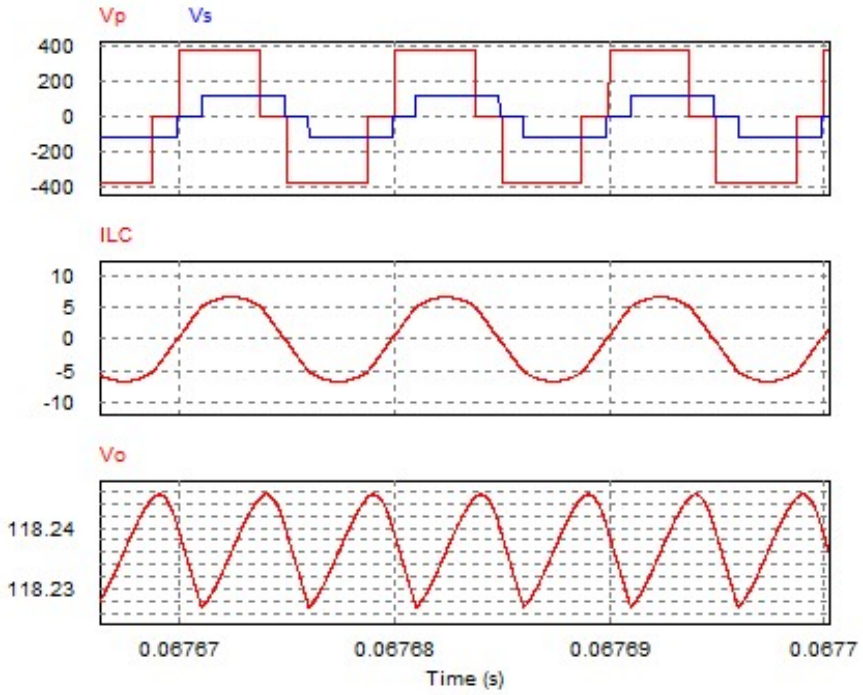

Fig. 7 Simulated waveforms of v_p and v_s, resonant tank current i_{LC}, output volgage V_o for output power P_o=500W (V_{in}=380V, V_o=120V)

ISSN: 2710-0588

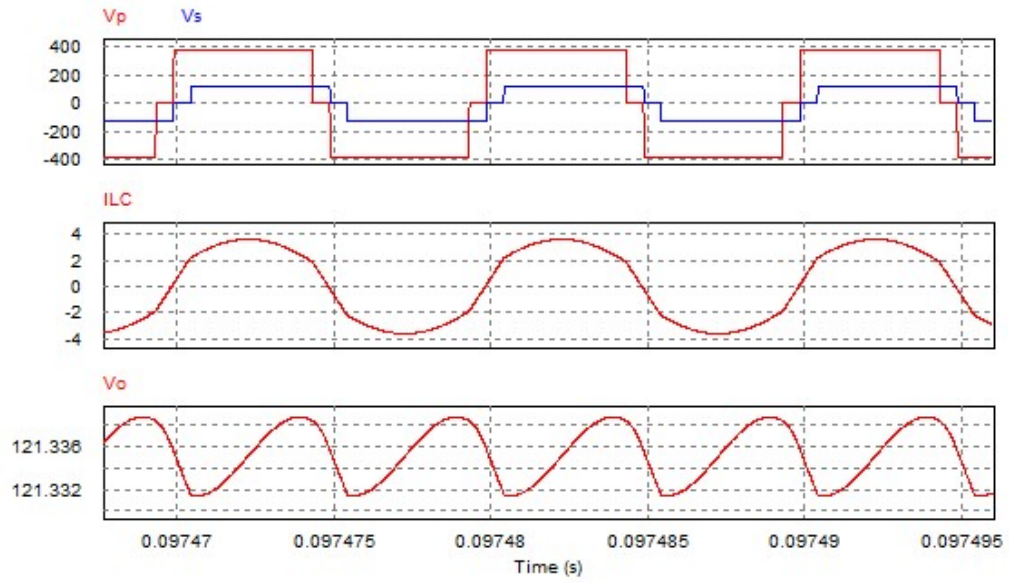

Fig. 8 Simulated waveforms of v_p and v_s, resonant tank current i_{LC}, output volgage V_o for output power P_o=300W (V_{in}=380V, V_o=120V)

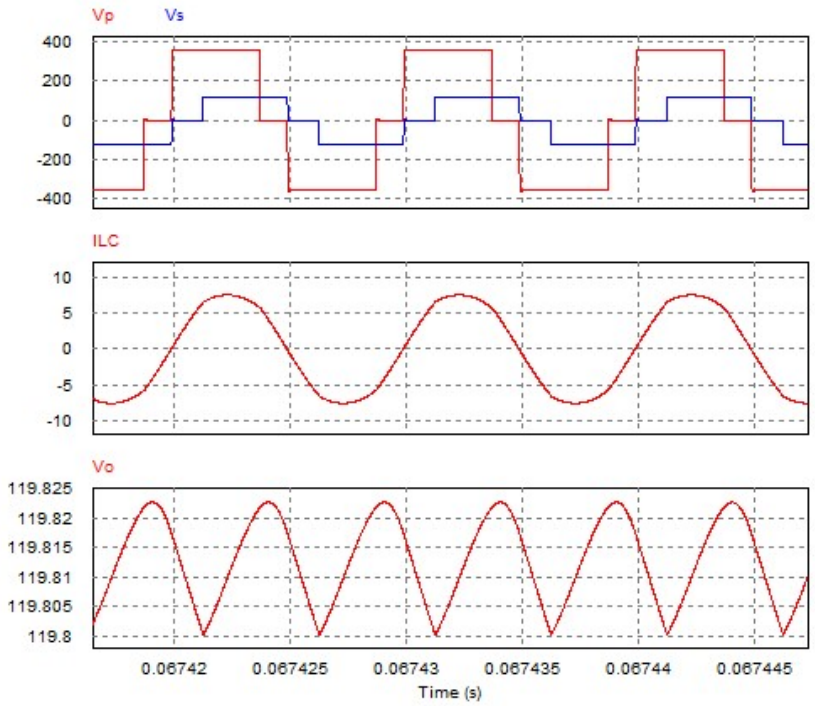

Fig. 9 Simulated waveforms of v_p and v_s, resonant tank current i_{LC}, output volgage V_o for output power P_o=500W (V_{in}=360V, V_o=120V)

ISSN: 2710-0588

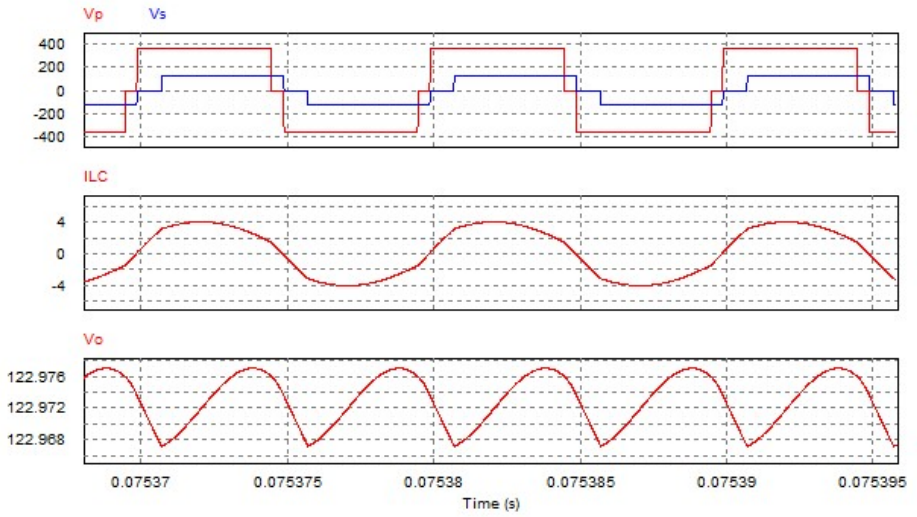

Fig. 10 Simulated waveforms of v_p and v_s, resonant tank current i_{LC}, output volgage V_o for output power P_o=300W (V_{in}=360V, V_o=120V)

4.3. Experimental Results

A prototype converter with the same designed specifications was built and tested in the lab. The steady-state plots obtained from experiments are illustrated in Fig. 11, in which the full load and 40% load conditions of three different primary side voltage levels are investigated for charging mode. The measured voltages and currents demonstrate good match with the simulation and theoretical results.

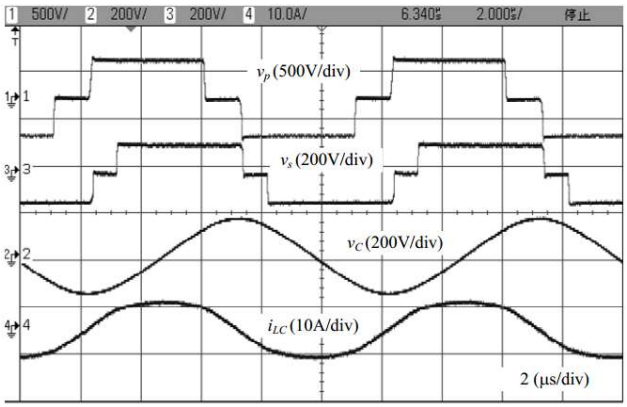

(a)

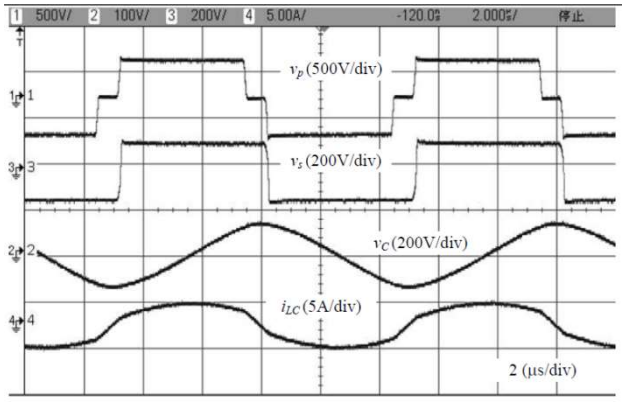

(b)

ISSN: 2710-0588

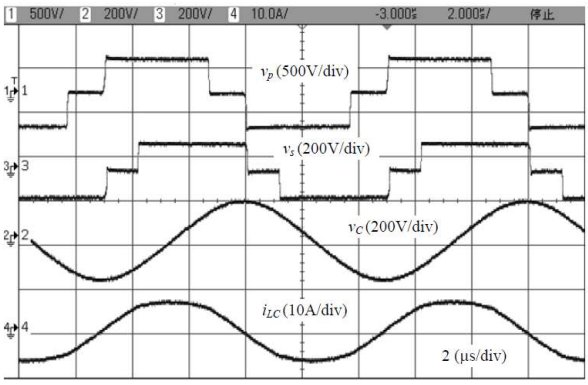

(c)

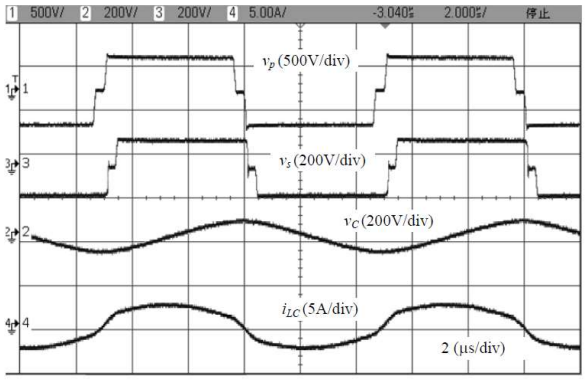

(d)

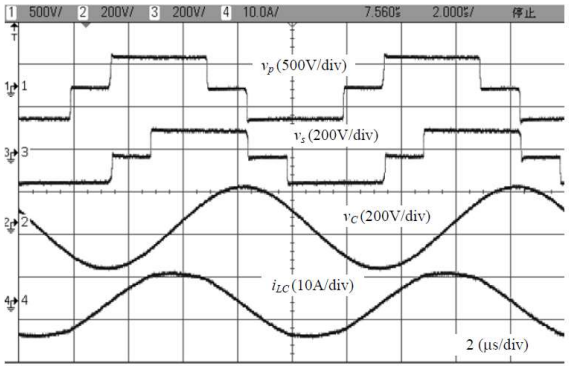

(e)

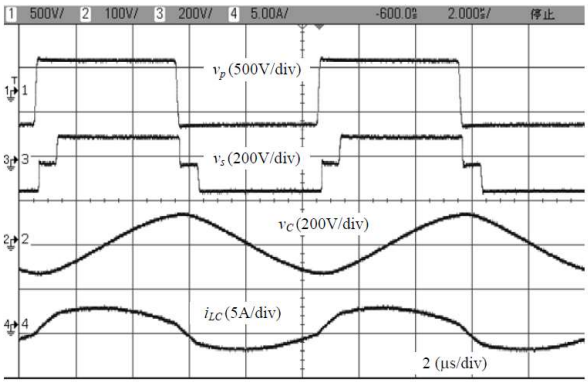

(f)

Fig. 11 Experimental steady-state plots at different voltage and output power (from top to bottom: primary HF ac voltage v_p, secondary HF ac voltage v_s, resonant tank capacitor voltage v_c and resonant tank current i_{LC}): (a) V_{in}=400V, Vo=120V, Po=500W. (b) V_{in}=400V, Vo=120V, Po=200W. (c) V_{in}=380V, Vo=120V, Po=500W. (d) V_{in}=380V, Vo=120V, Po=200W. (e) V_{in}=360V, Vo=120V, Po=500W. (f) V_{in}=360V, Vo=120V, Po=200W.

ISSN: 2710-0588

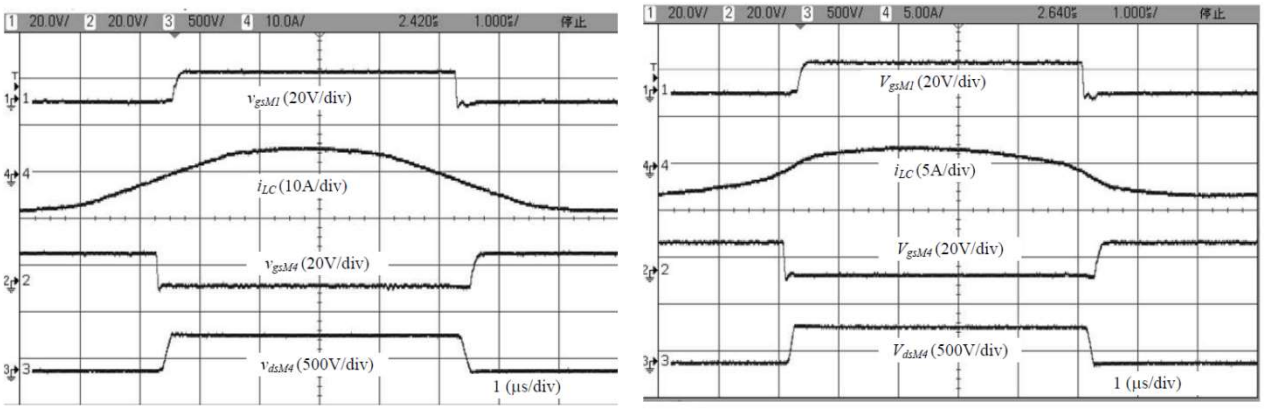

(a) (b)

Fig. 12 Experimental switching waveforms of primary side switches M_1 and M_4 (from top to bottom: driver signal v_{gsM1}, resonant tank current $i_{LC,}$ driver signal v_{gsM4}, drain to source voltage v_{dsM4}): (a) V_{in}=380V, Vo=120V, Po=500W. (b) V_{in}=380V, Vo=120V, Po=200W.

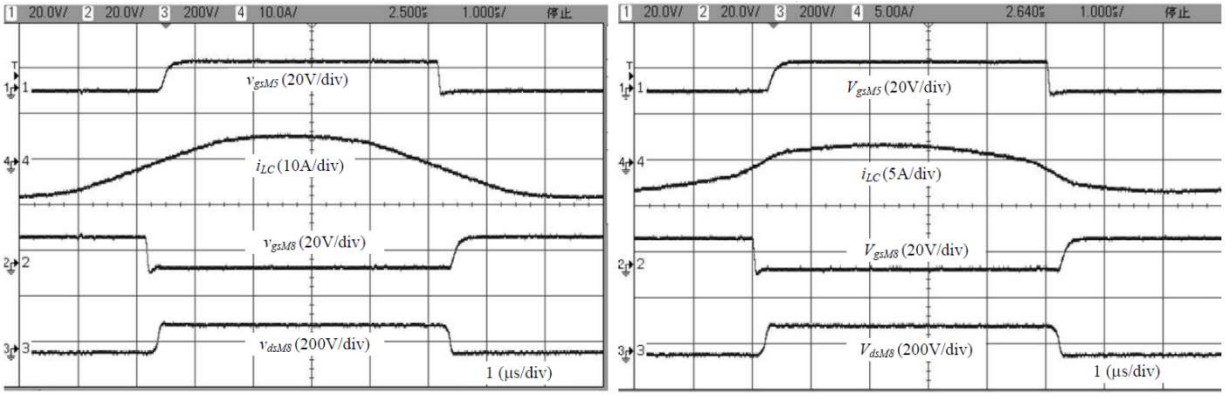

(a) (b)

Fig. 13 Experimental switching waveforms of secondary side switches M_5 and M_8 (from top to bottom: driver signal v_{gsM5}, resonant tank current $i_{LC,}$ driver signal v_{gsM8}, drain to source voltage v_{dsM8}): (a) V_{in}=380V, Vo=120V, Po=500W. (b) V_{in}=380V, Vo=120V, Po=200W.

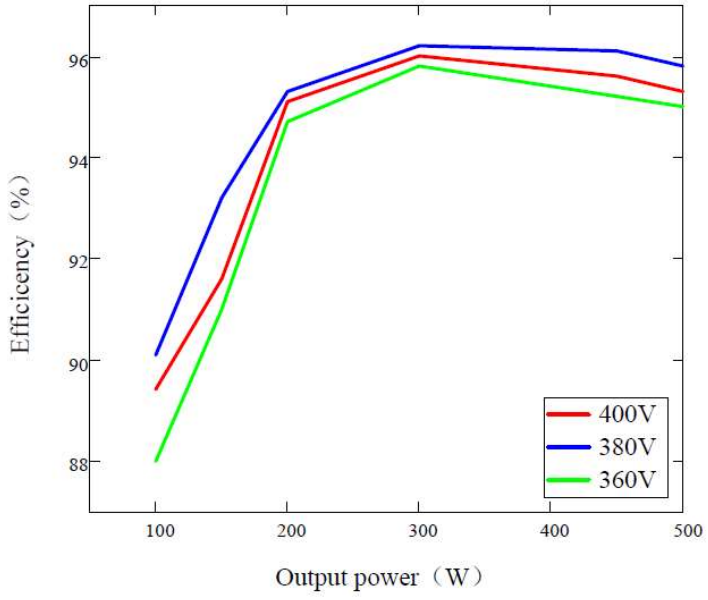

Fig. 14 Measured converter efficiency curves at different output powers and input voltages

ISSN: 2710-0588

The switching waveforms obtained from experiments are shown in Fig. 12-13, in which the full load and 40% load conditions of 380V input voltage are tested for charging mode. It can be seen that ZVS performance are achieved for the primary side leading legs switches M4 and the secondary side lagging legs switches M8. Meanwhile, the ZCS performance is achieved for the switches M1 and M5. The measured switching waveforms verify the simulation and theoretical results.

The measured converter efficiency curves obtained is shown in Fig. 14. At the full load condition, the measured efficiency are 95.3%, 95.8 % and 95.0% for Vin =400V, Vin =380V, and Vin =360V respectively. The peak efficiency of the proposed control can reach 96.1% .The efficiency of the converter is kept over 88% for load level over 20% rated output power.

5. Summary

In this paper, TPS gating scheme is applied to DBSRC and a unified boundary TPS control is proposed to minimize the circulating current and improve the overall converter efficiency. A physical converter is built for validation test. It can be concluded that with minimum circulating current control as the objective, the control scheme have better performance at a wide range of operation condition. With the variations of input voltage and output power, the unified boundary TPS control have high efficiency and low resonant current.

Acknowledgments

This work was supported by the Guangdong Provincial University Characteristic Innovation Project (Grant No. 2023KTSCX368) and School Level Scientific Research Project of Zhongshan Polytechnic (Grant No. KYB2405).

References

[1] S. Falcones, X. Mao, and R. Ayyanar. Topology comparison for solid state transformer implementation. Power and Energy Society General Meeting, 2010 IEEE. IEEE, 2010, pp.1–8.

[2] X. Li and A. K. Bhat. Analysis and design of high-frequency isolated dual-bridge series resonant dc/dc converter. IEEE Trans. on Power Electronics, vol. 25, no. 4, pp. 850–862, 2010.

[3] R. W. De Doncker, D. M. Divan, and M. H. Kheraluwala. A three-phase soft-switched highpower-density dc/dc converter for high-power applications. IEEE Transactions on Industry Applications, vol. 27, no. 1, pp. 63–73, 1991.

[4] X. Li. A llc-type dual-bridge resonant converter: Analysis, design, simulation, and experimental results. IEEE Transactions on Power Electronics, vol. 29, no. 8, pp. 4313–4321, 2014.

[5] V.Vorperian. Simplified analysis of PWM converters using the model of the PWM switch:parts Ⅰ and Ⅱ. IEEE Trans. on Aerospace and electronic systems, vol. AES-26, p. 490-505,1990.

[6] Mahafzah, K.A.; Obeidat, M.A.; Al-Shetwi, A.Q., et al. A Novel Synchronized Multiple Output DC-DC Converter Based on Hybrid Flyback-Cuk Topologies. Batteries 2022, 8, 93.

[7] B. Zhao, Q. Song, W. Liu, and Y. Sun. Overview of dual-active-bridge isolated bidirectional dc–dc converter for high-frequency-link power-conversion system. IEEE Transactions on Power Electronics, vol. 29, no. 8, pp. 4091–4106, 2014.

[8] B. Zhao, Q. Song, W. Liu, G. Liu, and Y. Zhao. Universal high-frequency-link characterization and practical fundamental-optimal strategy for dual-active-bridge dc-dc converter under pwm plus phase-shift control. IEEE Transactions on Power Electronics, vol. 30, no. 12, pp. 6488–6494, 2015.